Growth mechanism and dynamics of in-plane solid-liquid-solid silicon nanowires

Linwei Yu and Pere Roca i Cabarrocas

Laboratoire de Physique des Interfaces et des Couches Minces (LPICM), Ecole Polytechnique,
CNRS, 91128 Palaiseau, France

In this paper, we investigate the growth mechanism and dynamic behavior of in-plane solid-liquid-solid (IPSLS) silicon nanowires (SiNWs), mediated by indium drops which transform hydrogenated amorphous silicon into crystalline SiNWs. Two distinctive growth modes of the SiNWs have been identified: (1) the grounded-growth (GG) mode in which the produced SiNWs are fixed to the substrate and (2) the suspended-growth (SG) mode where the SiNWs are carried by and move together with the catalyst drops. A comparative study of the SiNWs produced in SG and GG modes provides important insights into the IPSLS mechanism and reveals the unique growth balance condition in the moving SiNWs/catalyst drop system. For the GG-SiNWs, the interplay between the front absorption interface and the rear deposition interface of the catalyst drop leads to an interesting growth dynamics, which can be described by a kinetic equation model. For the SG-SiNWs, direct evidences of the *rolling-forward* behavior of the liquid catalyst drop have been witnessed.

I. INTRODUCTION

Silicon nanowires (SiNWs) are the elemental building blocks for future nanodevices[1,2] and are promising to push forward the device miniaturization while preserving the compatibility to the full-fledged Si technology. The novel electronic,[1,3] optical,[4] and thermoelectric[5] properties of SiNWs provide the basis for developing a new generation of high-performance nanodevices.[3,6] Several growth mechanisms have been proposed and successfully used to obtain well-defined SiNWs, for example, the vapor-liquid-solid (VLS),[7–12] oxide-assisted growth,[13,14] solid-liquid-solid (SLS),[15] and solution-liquid-solid[16] growth modes. In the well-known VLS mode, the gas precursors (such as SiH_4) are dissociated on the surface of catalyst droplets, such as Au,[7] Al,[17] Cu,[18] Sn,[19] or In,[20] then the Si atoms are absorbed, transported, and precipitated as crystalline SiNW. In the SLS mode,[15,21] the SiNWs can be produced from a crystalline Si wafer by using nickel as catalyst, which however requires a rather high reaction temperature ($\sim 1000\ ^\circ$C).

Recently, we proposed and demonstrated an in-plane SLS (IPSLS) growth mode for obtaining an in-plane growth of SiNWs, where a nanoscaled liquid indium droplet catalyzes the growth of SiNWs by consuming and transforming hydrogenated amorphous silicon (a-Si:H) into crystalline SiNW, in an all *in situ* and reactive-gas-free annealing process.[22] From an application point of view, this in-plane growth of SiNWs could provide new opportunities for designing and exploiting various SiNW-based nanodevices, in a way more compatible with the established planar Si architecture. Intrinsically, this IPSLS growth mode can be viewed as a nanoscaled metal-induced crystallization[23–25] or a nanoscaled liquid-phase-epitaxy[26,27] process. In contrast to its *bulk versions*, this nanoscale crystallization process produces well-defined nanowires with controllable size, morphology, and even growth path.[22,28] Compared to the VLS mode, a unique aspect of the IPSLS process is that both the front (absorption) and the rear (deposition) interfaces in the catalyst drop are liquid/solid interfaces, and the movements of these two *hard*

interfaces (in contrast to the top soft gas/liquid interface in the VLS mode) are always coupled to each other via the liquid catalyst drop. In case of a speed difference between the two interfaces, the catalyst drop will be deformed (stretched or squeezed) and lead to rich dynamic behavior. We have shown that this interplay can be effectively controlled and utilized to *tailor* the morphology of the produced SiNWs.[22,28] Here, we present a detailed study on the growth mechanism and the dynamic behavior of the SiNWs obtained via IPSLS mechanism in order to set a basis for obtaining a comprehensive understanding of this growth process.

II. EXPERIMENTS

The experimental steps for fabricating SiNWs in IPSLS mode include: (1) first, the formation of In catalyst drops directly on top of indium tin oxide (ITO) coated glass substrates by using a H_2 plasma treatment with a typical rf power, H_2 flow rate, and chamber pressure of 5 W, 100 SCCM (SCCM denotes cubic centimeter per minute at STP), and 600 mTorr, respectively, at 300 $^\circ$C for 1 min; (2) second, the deposition of a thin layer of a-Si:H (H_a =10–50 nm) by the dissociation of pure SiH_4 under the following conditions: rf power, SiH_4 flow rate, and chamber pressure of 2 W, 10 SCCM, and 120 mTorr at 100 $^\circ$C, respectively; and (3) third, the annealing of the samples in vacuum ($<10^{-6}$ mbar) at T_{sub}=300–500 $^\circ$C, to activate the In catalyst drops to absorb the a-Si:H layer and produce crystalline SiNWs behind. This fabrication process is briefly illustrated in Figs. 1(a)–1(c). A series of samples with different a-Si:H covering thickness (H_a) and growth temperatures (T_{sub}) were prepared and summarized in Table I. The a-Si:H layer deposited under the above condition covers conformally and uniformally on both the In catalyst drops and the flat surface region. The thickness of the a-Si:H covering layer was determined from spectroscopic ellipsometry measurements (on a codeposited Cg substrate). The substrate temperatures were measured by a thermocouple directly attached to the sample holder. The SiNWs were characterized
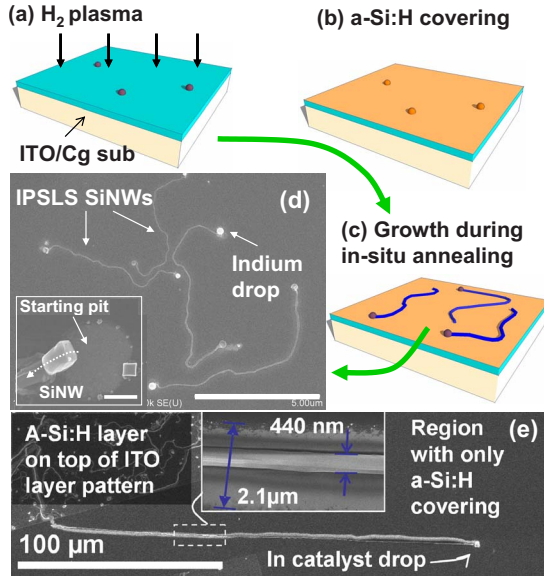
FIG. 1. (Color online) [(a)–(c)] Schematic illustrations of the fabrication steps of the IPSLS SiNWs; (d) SEM image of typical SiNWs, with the inset providing an enlarged view of the starting pit of a SiNW with a detached initial segment; (e) a long and straight SiNW growing out from the a-Si:H/ITO pad into the region with only a-Si:H covering the glass substrate. A close view of the SiNW segment is provided in the inset. The scale bars in (d) and the insets of (d) and (e) are 5 μm, 300 nm, and 100 μm, respectively.

by using scanning electron microscopy (SEM, Hitachi S4800), and the length and diameters of the SiNWs and their corresponding catalyst drops were measured from the SEM observations. Except mentioned otherwise, the SEM images used for measuring the dimensions of the SiNWs were taken in top view.

III. RESULTS AND DISCUSSIONS

A. Different growth modes of IPSLS SiNWs

In Fig. 1(d), we show a SEM image of in-plane SiNWs obtained via the IPSLS growth mechanism (sample F in Table I, with an a-Si:H covering layer thickness of H_a =17 nm after annealing at T_{sub}=500 °C). The growth of SiNWs is mediated by In catalyst drops, which can be clearly

TABLE I. A brief summary of the different a-Si:H covering layer thicknesses and the annealing temperatures for obtaining of a series of IPSLS SiNWs samples.

Sample no.	a-Si:H thickness (H_a) (nm)	Annealing temperature (T) (°C)
A	17	350
B	17	400
C	10	450
D	17	450
E	34	450
F	17	500
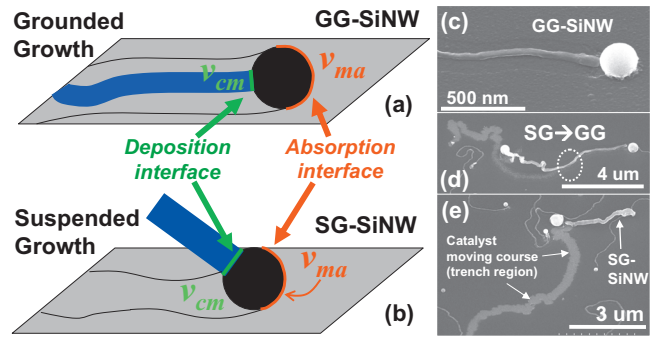
FIG. 2. (Color) Schematic illustrations of the two different growth modes for the growth of IPSLS SiNWs: (a) the GG mode with SiNWs being attached to the substrate surface and (b) the SG mode with SiNWs being suspended and carried by the catalyst drop. (c) and (e) present the corresponding SEM pictures of the GG-SiNWs and SG-SiNWs, respectively. A transient case, from the initial SG mode to the final GG mode during the growth, is also shown in (d).

distinguished in the SEM picture as the bright spots at the end of the SiNWs. Shallow trench regions along with the SiNWs can be seen (in a lower contrast), which were formed by the In drops when they consumed and thinned the local a-Si:H layer during growth. The crystallinity of the as-produced SiNWs has been examined and confirmed by using a local Raman setup.[22] According to the experimental observations, two distinct growth modes could be found for the IPSLS SiNWs: (1) the grounded-growth (GG) mode in which the produced SiNWs are attached to the substrate surface, as shown by the schematic illustration and the typical SEM image in Figs. 2(a) and 2(c), respectively, and (2) the suspended-growth (SG) mode in which the produced SiNWs are suspended and carried by the catalyst drop during its movement, as depicted in Figs. 2(b) and 2(e), respectively. Meanwhile, transient cases from the SG mode to the GG mode (during the growth of the SiNWs) were observed as shown, for example, in Fig. 2(d). In both growth modes, as illustrated in Figs. 2(a) and 2(b), the Si atoms are absorbed from the a-Si:H matrix at the front In/a-Si:H interface and then precipitated at the rear SiNW/In interface. An interesting point to note is that, in the GG mode, the speed (v_{ma}) of the front interface is coupled to the speed of the rear interface (v_{cm}) via the liquid catalyst drop while in the SG mode these two interfaces are decoupled since the produced SiNWs are suspended and carried by the catalyst drop. This situation provides an important comparative view point for understanding the growth mechanism of the IPSLS SiNW and will be discussed later.

As in the VLS growth mode,[7–10] the average diameter of the produced SiNWs is determined by the diameter of the *leading* In catalyst drop. As shown in Fig. 3, the diameter of SiNWs (R_w) is found to be proportional to the diameter of their guiding In drops (R_c), with their cross-section-area ratio $f \equiv R_w^2/R_c^2$ being approximately a constant. This proportionality seems to be independent of both the thickness of the a-Si:H layer and the growth temperature (within the range of current experimental conditions). The deviation from this linear relation is found to broaden with the increase in the cata-
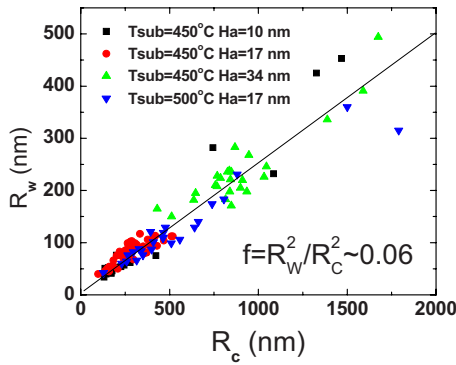
FIG. 3. (Color online) Relation between the diameter of the In catalyst drop (R_c) and the diameter of the produced SiNWs (R_w) for different a-Si:H covering thickness (H_a) and annealing temperatures (T_{sub}).

lyst diameter. This could arise from the unique situation for the liquid catalyst in the IPSLS mode, where the catalyst drop is usually subject to distortions caused by the dynamic interplay between the two solid/liquid interfaces of the catalyst drop (that is, the front SiNW/In interface and the rear In/a-Si:H interface), as will be discussed later in more details.

In the following, the velocity of the In(metal)/a-Si:H interface (v_{ma}) in both the GG and SG modes is defined as the moving rate of the catalyst (or the advancing speed of the wire-catalyst system), which is obtained by dividing the total trench length by the total annealing time. In the GG mode, the growth rate of SiNW, v_{cm} of the c-SiNW/In (metal) interface, is on average the same as the moving rate of front interface, that is $v_{cm}=v_{ma}$; in the SG mode, the SiNWs are found to be shorter than the total trench length traveled by the catalyst drop (thus $v_{cm}<v_{ma}$) and to have a irregular morphology. In Fig. 4, we present the dependence of the moving rate of catalyst drops (v_{ma}) on the diameter of the SiNWs (R_w, which is proportional to the diameter of catalyst drop R_c), for various thicknesses of the a-Si:H layer and for different growth temperatures.

According to the SEM observations, two regimes (as indicated by the dash lines) in Fig. 4 can be distinguished for the growth of SiNWs in GG mode or in SG mode. We found that the SG growth mode, as shown in Figs. 2(d) and 2(e), is usually adopted by the larger catalyst drops while the GG growth mode is more common among the smaller SiNWs. Meanwhile, the SG mode is more likely to happen during the initial growth stage, as can be seen for the transient cases, where the SiNWs start in SG mode and then switch to GG mode [in Fig. 2(d)]. This observation seems to indicate that a short segment of SiNW will be more easily carried by a large catalyst drop. Further analysis also indicates that the occurring of SiNWs in SG mode is related to the following aspects: (1) as compared to small catalyst drops, a large catalyst drop offers a higher position for the produced SiNW segment to be kept away from the substrate and is able to *carry* a SiNW segment (especially during its early growth stage).

(2) During the initial stage of the IPSLS process, the SiNW segment could be disconnected from the substrate sur-
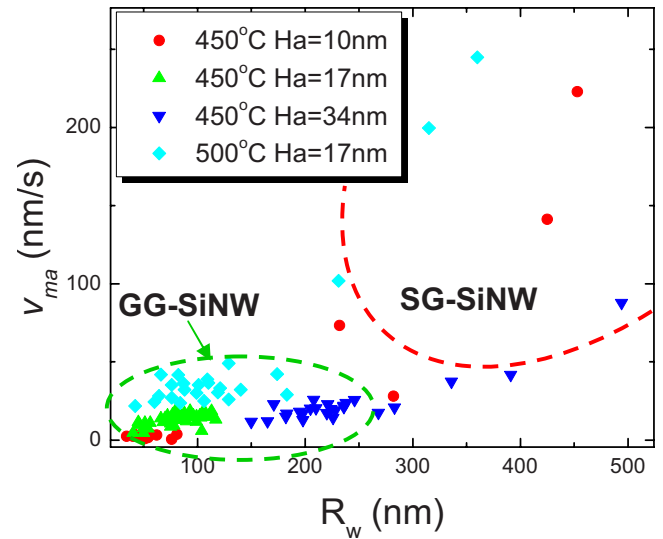
FIG. 4. (Color online) The dependence of the moving rate of catalyst drops (v_{ma}) on the diameter of the SiNWs (R_w) for various thicknesses of the a-Si:H covering layer and at different growth temperatures. According to the SEM observations, two regimes, as indicated by the dash lines, respectively, can be distinguished for the growth of SiNWs in GG mode or in SG mode, respectively.

face, as shown, for example, by the inset of Fig. 1(d). As discussed in our previous study about the initial nucleation of the IPSLS SiNWs,[29] the lateral growth of the catalyst is usually triggered by the largest nucleation center formed around the bottom edges of the catalyst drop. Then, a new absorption interface between the catalyst drop and the a-Si:H layer is formed and draws the In catalyst into a lateral movement.[29] During this process, a rupture of the early SiNW segment from its nucleation center (detached from the substrate) could happen. This provides the initial SG condition for the following growth of SiNWs.

In comparison to the GG-SiNWs, the SG-SiNWs usually feature an irregular moving course, as seen in Figs. 2(d) and 2(e). This phenomenon results from the fact that the suspended SiNW segment *carried by* the catalyst drop could cause random perturbations to the movement of the catalyst drop and distort its moving course. This is in contrast to the GG-SiNWs where the SiNWs behind (attached to the substrate) help to stabilize the advancing direction of the catalyst drops.

Interestingly, since the two liquid/solid interfaces in the SG mode are decoupled, the SG-SiNWs provide a "*simplified*" situation and a *comparative view point* for understanding the IPSLS growth mechanism. In particular, it allows us to (1) focus on the effect of the front a-Si:H/In absorption interface and (2) gain insight on the mass transport through the catalyst (as discussed below). First of all, the SG-SiNWs provide a straightforward evidence for the existence of an *independent drawing force* at the front a-Si:H/In interface since the SiNWs are carried by the catalyst drops and there is no other force exerting or pushing from behind. As discussed before,[22] the drawing force arises from the imbalanced forces exerted at the triple-phase line (where the liquid In drop, a-Si:H and vacuum join). As the a-Si:H matrix is continu-
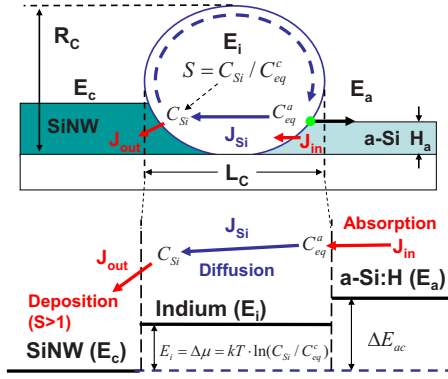
FIG. 5. (Color online) Schematic illustration for the absorption, diffusion, and deposition steps involved in the growth of lateral SiNW via IPSLS mechanism. E_a, E_c, and E_i denote the Gibbs energy of Si atoms in the amorphous, crystalline, and dissolved (in In catalyst drop) states, respectively; C_{Si} is the dissolved Si atom concentration in the catalyst drop; J_{in}, J_{out}, and J_{Si} are the absorption, deposition, and mass transport (diffusion) flux rates of Si atoms.

ously consumed by the catalyst drop, there is a net force exerted at the triple-phase line, which draws the catalyst *toward* the a-Si:H matrix. Meanwhile, the bulk interface between the liquid indium and the a-Si:H matrix can also contribute to the drawing force exerted on the liquid catalyst drop. The existence of a drawing force at the a-Si:H/In interface can be directly inferred from the initial movement of the catalyst drop during its start-up process (when the triple-phase line has not yet been formed).[29] The detailed mechanism and nature of these driving forces is still an open field, and the following discussions and models will focus on the fact that the catalyst/SiNW is driven by a combined drawing force at the front absorption interface. Meanwhile, it is indeed remarkable that, as seen in Figs. 2(d) and 2(e), the carried SiNW segments can be as long as several micrometers with a diameter of a few hundred nanometers, indicating that the drawing force at the absorption interface is indeed strong to drive not only the large liquid catalyst but also the SG-SiNWs on top.

B. Growth steps of SiNWs via IPSLS mechanism

The growth of SiNWs in IPSLS mechanism can be viewed as a nanoscaled solid-state crystallization process, driven by a Gibbs energy difference between the a-Si:H (E_a) and crystalline SiNW (E_c) as indicated in Fig. 5, with $\Delta E_{ac} = E_a - E_c \approx 0.12 – 0.15$ eV.[30,31] The In catalyst drops absorb Si atom from the *solid-state precursor* of a-Si:H and deposit it as the crystalline SiNW. As depicted in Fig. 5, the major growth steps involved in the IPSLS process include: (i) the dissociation and absorption of Si atoms from the a-Si:H matrix into the In catalyst drop at the front a-Si:H/In interface; (ii) the mass transport of the dissolved Si atoms across the In catalyst; and (iii) the deposition of Si atoms on the SiNW side at the rear SiNW/In interface. Putting aside the solid-state precursors, these major growth steps are similar to those involved during the VLS growth mode. Compared to the gas precursor dissociation process in the VLS growth mode, the

dissociation energy of Si-Si bonds in the a-Si:H matrix is energetically less demanding than the Si-H bond breaking process (in the case of dissociation of SiH$_4$) in VLS mode. Moreover, the Si atom density in the solid-state a-Si:H film is several orders of magnitude higher than that achievable in the case of gas precursors in VLS mode. These two factors combined enable a quicker dissociation and absorption process of Si atoms at the a-Si:H/In interface. As we can see in Fig. 4, the moving rate of SG-SiNWs is much faster than that of GG-SiNWs. This reflects that the Si-Si dissociation process at the a-Si:H/In interface is not limiting the moving rate of the SiNW-catalyst system and is indeed a quick enough process. This bond dissociation process is only relevant to the intrinsic properties at the a-Si:H/In interface and should not be the rate-limiting factor here, otherwise no size or growth mode dependence should be observed for the moving rate.

From a microscopic viewpoint, the mass transport of dissolved Si atoms in the In catalyst is driven by the different Si equilibrium concentrations seen by the two liquid-solid interfaces, that is, at the front a-Si:H/In interfaces and at the rear SiNW/In interface. Specifically, since the Gibbs energy of Si atoms in a-Si:H ($\Delta E_{Si} = E^a_{Si} - E^c_{Si}$) is higher than that in SiNW, the equilibrium dissolved Si atom concentration at the a-Si:H/In interface ($C^a_{eq} = C^c_{eq} \cdot e^{\Delta E_{ac}/kT}$) is thus higher than that at the SiNW/In interface (C^c_{eq}). As indicated in Fig. 5, if the Gibbs energy of Si atom in the crystalline SiNW is taken as a reference, the chemical potential of the dissolved Si atoms in the In catalyst drop (E_i) can be written as[32]

$$\Delta \mu = E_i - E_c = kT \ln S = kT \ln(C_{Si}/C^c_{eq}), \qquad (1)$$

where $S \equiv C_{Si}/C^c_{eq}$ is the supersaturation state in the In catalyst with respect to the SiNW/In interface, C_{Si} is the Si concentration at the SiNW/In interface (with $C^a_{eq} \geq C_{Si} > C^c_{eq}$) while k and T are the Boltzmann constant and the substrate temperature, respectively.

The coexistence of these two liquid/solid interfaces in the same liquid catalyst drop means that a supersaturation state of dissolved Si atoms, with respect to the c-Si/In interface, can be established and sustained by the Si atoms absorbed from the a-Si:H/In interface, with

$$S = C_{Si}/C^c_{eq} = e^{\Delta \mu/kT}. \qquad (2)$$

It is important to note that the maximum supersaturation state S_{max}, that can be reached in the In catalyst, is also limited by ΔE_{ac} and can be estimated (at $T_{sub} \sim 500\ °C$) to be around

$$S_{max} = C^a_{eq}/C^c_{eq} = e^{\Delta E_{ac}/kT} \approx 6.1 – 9.5. \qquad (3)$$

During the growth of IPSLS SiNWs, the Si atoms are absorbed at the front a-Si:H/In interface and then transported to the rear SiNW/In deposition interface via a diffusion process. Considering that the dissociation of Si atoms from a-Si:H matrix is a quick step as explained before, the incorporation rate of Si atoms from the a-Si:H matrix (J_{in}) into the catalyst drop is thus determined by the diffusion transport flux (J_{Si}) across the catalyst drop, which is given as

$$J_{in} = J_{Si} = D_s(C_{eq}^a - C_{Si})/L_c = D_s(C_{eq}^c \cdot e^{\Delta E_{ac}/kT} - C_{Si})/L_c, \quad (4)$$

with L_c defined as the length of the catalyst drop, as indicated in Fig. 5, and D_s is the diffusion coefficient of Si atom in the In catalyst. The implication of this point on the growth rate and dynamics of the IPSLS SiNWs will be discussed in detail later. As discussed in our previous work,[22] the concentration difference ΔC_{Si} across the In catalyst, needed for sustaining a growth rate of 10^2 nm/s, accounts for only a very small portion of the equilibrium concentration ($\Delta C_{Si}/C_{eq}^c$ $<2\%$ at $400-500$ °C), that is, in most cases, C_{Si} can be considered to be very close to C_{eq}^a. This situation can also be inferred from the observation that the full thickness of the a-Si:H layer in the trench region of GG-SiNW is not always totally absorbed. In these cases, the high Si concentration in the In catalyst drop limits the absorption process and therefore the a-Si:H layer is only partially consumed.

With a supersaturation state of dissolved Si atoms built up at the SiNW/In interface, the deposition of Si atoms on the SiNW end can be readily described based on the well-established theoretical framework for the growth of VLS SiNWs.[33–35] The interface between the SiNW and the In catalyst drop is usually terminated with the energetically stable planes of Si(111), Si(110), and Si(100). The growth of a new Si monolayer on these stable planes requires first the formation of new two-dimensional (2D) nucleation center on these planes and then a lateral growth of a new complete Si monolayer. According to the nucleation rate theory in VLS mode,[33,34] this outgoing (deposition) flux rate J_{out} is given by

$$J_{out} \sim G_{nc}^{-1/2} \cdot e^{-G_{nc}/kT} \quad (5)$$

with $G_{nc} = \pi \cdot \gamma^2 \cdot \Omega^{4/3}/\Delta\mu$ being the nucleation barrier for the formation of 2D nucleation centers on the SiNW end.

C. Growth rate and balance conditions for IPSLS SiNWs

A close scrutiny of Fig. 4 reveals several general trends for the size dependence of the moving rate of SiNWs: (1) the SG-SiNWs have a faster moving rate than that of GG-SiNWs and (2) among the SG-SiNWs, the moving rate tends to increase significantly with the size of the SiNWs R_w (that is, also with the size of the catalyst drop R_c). (3) For the GG-SiNWs, the moving rate seems to "*increase*" slightly with the size of the SiNWs. However, the amount of increase is smaller than the statistical data uncertainty. This situation and the large uncertainty could be attributed to the fact that the statistic data were sampled through postgrowth SEM characterizations, which are influenced by the bending morphology of the wires (which could lead to an underestimation of the actual length since only the course length is measured for calculating the moving rate). In order to obtain a direct measurement of the size dependence of the GG-SiNWs, a real-time SEM characterization was performed. This is enabled by the unique reacting-gas-free growth process of the IPSLS SiNWs, where a high-vacuum environment required by the SEM measurements can be maintained during the annealing process. The sample prepared for the real-time SEM measurement has a H_2 plasma treatment time of 3 min
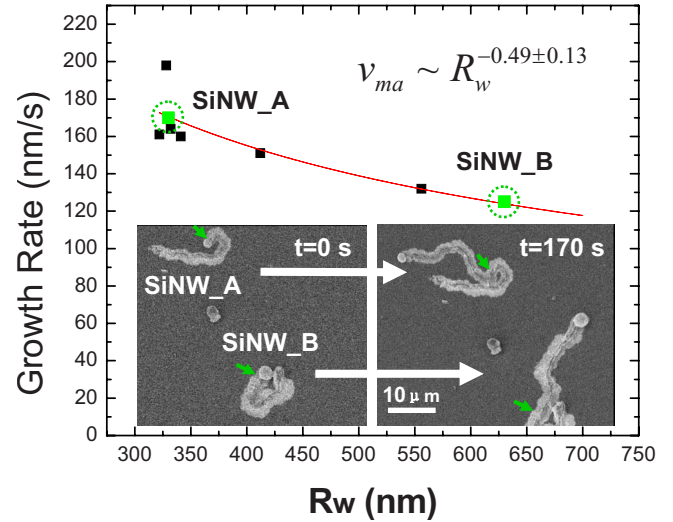
FIG. 6. (Color online) The growth rate of the SiNWs as a function of their diameter as deduced from *in situ* real-time SEM observation. The two insets show the SEM images of two growing GG-SiNWs with different diameters ($R_{wA} \approx 330$ nm and R_{wB} ≈ 630 nm), captured at $t=0$ s and $t=170$ s, respectively. The starting points for the measurement are indicated by the short green (light gray in print) arrows.

and a thicker a-Si:H covering layer of $H_a = 51$ nm. As shown by the two insets in Fig. 6, two SiNWs growing in GG mode with different diameters ($R_{wA} \approx 330$ nm and $R_{wB} \approx 630$ nm) can be seen simultaneously during an annealing at ~ 550 °C. The starting places ($t=0$ s) are marked by the short green (light gray in print) arrows in both the SEM pictures. The corresponding growth/moving rates of these two SiNWs are highlighted as the green spots in the plot shown in Fig. 6, as well as those data from other *in situ* real-time SEM measurements. As we can see, the moving rate shows actually a slowly decreasing trend with the increase in the diameter of SiNWs.

During the growth of GG-SiNWs, the front absorption and rear deposition interfaces of the catalyst drop need to develop at the same moving rate $v_{cm} = v_{ma}$. Otherwise, the liquid catalyst drop will be subject to distortions. As illustrated in Fig. 7(a), the absorption flux rate of Si atoms from the a-Si:H matrix $J_{in} = v_{ma} \cdot \alpha/\Omega$ is, according to Eq. (4), driven by a diffusion process and has a maximum flux rate of $D_s(C_{Si}^a - C_{Si}^c)/L_c$ (or a zero minimum) when $C_{Si} = C_{Si}^c$ (or $C_{Si} = C_{Si}^a$) while the deposition flux rate on the SiNW end $J_{out} = v_{cm}/\Omega$ increases with C_{Si} [but not linearly as learnt from Eq. (5)] and is zero when $C_{Si} = C_{Si}^c$ (no supersaturation of Si atom). In a balanced growth of a GG-SiNW, these two flux rates should be equal $J_{in} = J_{out}$ (at least on average), as marked by the green (gray in print) dot at the intersection of these two curves in Fig. 7(a). This equilibrium point also determines the Si atom concentration in the catalyst C_{Si} and the growth rate of the GG-SiNW (defined as $v \equiv v_{ma}$ $= J_{in}\Omega\alpha^{-1}$). According to Eq. (4), the slope of the absorption flux rate (in GG mode) J_{in}^{GG} against the Si concentration C_{Si} is
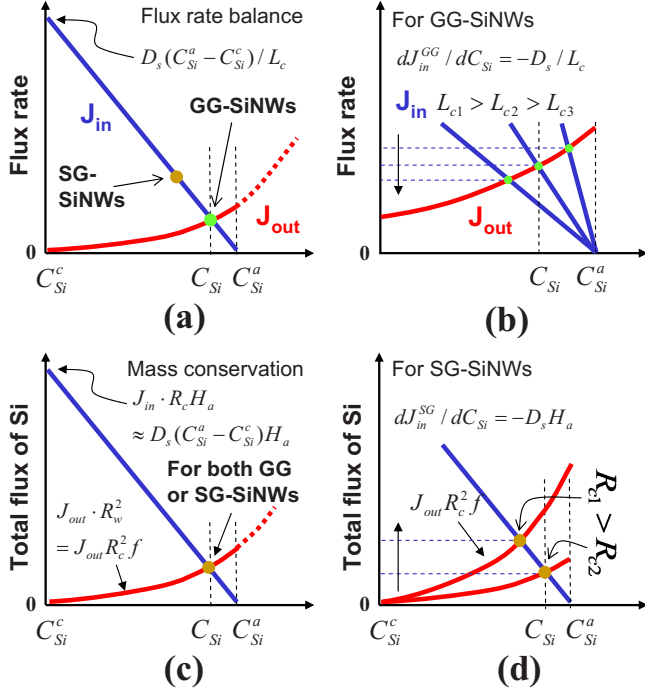
FIG. 7. (Color online) (a) The rate balance condition $J_{in}=J_{out}$ for the absorption $J_{in}=v_{ma}\cdot\alpha/\Omega$ and the deposition $J_{out}=v_{cm}/\Omega$ Si atom flux rates in the In catalyst drops, as a function of the dissolved Si atom concentration C_{Si}. (b) depicts the variation in the balanced condition in the catalyst drops (developing in GG mode) with different sizes of $L_{c1}>L_{c2}>L_{c3}$. (c) The mass conservation condition ($J_{in}R_cH_a=J_{out}R_w^2$) between the incoming and outgoing Si atoms in the In catalyst drops. (d) depicts the change in balanced condition for catalyst drops (developing in SG mode) with different sizes of $R_{c1}>R_{c2}$.

$$dJ_{in}^{GG}/dC_{Si}=-D_s/L_c. \tag{6}$$

Thus, both the Si concentration C_{Si} and the moving rate of the catalyst drop decrease monotonically with the increase in the size of catalyst drops. For instance, for catalyst drops of sizes of $L_{c1}>L_{c2}>L_{c3}$, we should have $C_{c1}<C_{c2}<C_{c3}$ and $J_{in1}^{GG}<J_{in2}^{GG}<J_{in3}^{GG}$, as illustrated in Fig. 7(b).

Meanwhile, according to the mass conservation condition during the growth, the Si concentration C_{Si} (at the deposition interface) in the catalyst is given by

$$V_c\frac{d}{dt}C_{Si}=J_{in}\cdot\alpha H_aR_c-J_{out}\cdot fR_c^2 \tag{7}$$

with V_c and α being the volume of the In catalyst drop and the volume contraction between the amorphous and crystalline silicon phases, respectively. During growth, C_{Si} can be considered as an average constant value and thus the total amount of incoming and outgoing Si atoms in the catalyst drop should also be balanced

$$J_{in}\cdot\alpha H_aR_c\approx J_{out}\cdot fR_c^2. \tag{8}$$

This mass conservation condition is depicted in Fig. 7(c), where the Y axis is the "total flux of Si," that is, the amount of Si atoms being absorbed or deposited per unit time at the
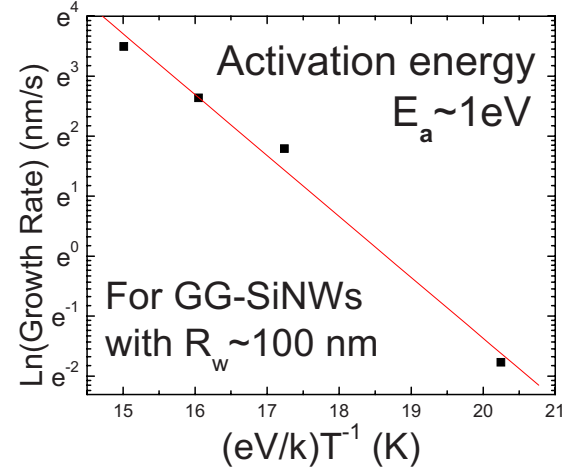
FIG. 8. (Color online) Arrhenius plot of the moving rate of GG-SiNWs (with similar diameter of 100 nm) against inverse temperature ($1/T$).

two interfaces. According to Eq. (4), the total incoming flux of Si atoms, the left term in Eq. (8), scales independent of the size of the catalyst since

$$J_{in}\cdot\alpha H_aR_c=D_s(C_{eq}^a-C_{Si})H_a\cdot R_c/L_c\approx D_s(C_{eq}^a-C_{Si})H_a. \tag{9}$$

And the total deposition flux term, the right-hand-side term in Eq. (8), scales with $\sim R_c^2$. Therefore, with the increase in R_c, the intersect point will move up along the basically unchanged absorption line, corresponding to a decrease in Si concentration and an increase in the absorption rate (the moving rate of the catalyst). This also explains the phenomenon that, as witnessed in Fig. 4, the moving rate is found to increase slightly with the increase in a-Si:H thickness H_a.

For the growth of GG-SiNWs, both the *flux rate balance* (to match the speeds of the two moving interfaces) and the *mass conservation* condition (to balance the absorbed and deposited Si atoms) have to be satisfied. This situation is specific to the IPSLS growth mechanism and does not apply to the VLS growth mode. Deviations from these two balanced conditions will result in a corresponding shape deformation of the liquid catalyst drop and cause the growth dynamics.

For the SG-SiNWs, the stringent requirement of $J_{in}=J_{out}$ is relaxed and only the mass conservation constraint is imposed. As depicted in Fig. 7(d), with the increase in the catalyst size of the SG-SiNW, the Si concentration in the catalyst decreases and the absorption rate of Si atoms from the a-Si:H matrix increases.

In Fig. 8, we present the temperature dependence of the growth rate of GG-SiNWs (with $v_{cm}=v_{ma}$), in an Arrhenius plot of the growth rate versus the inverse temperature ($1/T$). Since the growth rate depends on the size of catalyst drops and the a-Si:H covering layer thickness, we choose to compare the growth rate of SiNWs with a similar size of R_w ~ 100 nm. As can be seen, the growth rate of SG-SiNWs is thermally activated with an activation energy of ~ 1 eV, as deduced from the slope of the Arrhenius plot. This value is
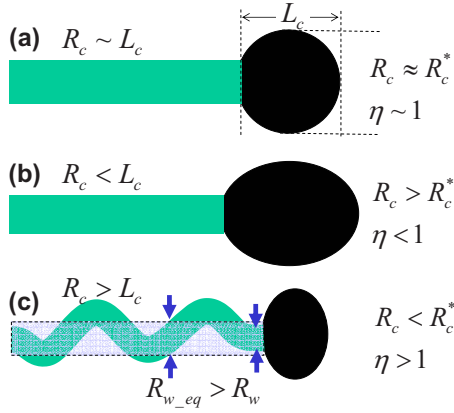
FIG. 9. (Color online) (a)–(c) depict the deformation situations of catalyst drops during growth in case of different catalyst sizes: $R_c \sim R_c^*$, $R_c > R_c^*$, and $R_c < R_c^*$, and thus $\eta \sim 1$, $\eta < 1$, and $\eta > 1$, respectively. For the case of $\eta > 1$, R_{w_eq} denotes the equivalent diameter of the SiNW if the bending SiNW is transformed into a straight but thicker one (with the same volume), with $R_{w\_eq} > R_w$.

much higher than the typical diffusion activation in liquid metal[36,37] and the activation energy of In catalyzed growth of SiNWs in VLS mode (~ 0.4 eV in plasma enhanced deposition according to our previous experiments on the vertical growth of SiNWs) (Ref. 38) but close to the activation energy reported in literature for the step of nucleation and deposition of Si atoms on the VLS SiNWs (0.8–1.3 eV).[39,40]

D. Growth dynamics and mechanism of IPSLS SiNWs

1. Interplay between the interfaces in GG-SiNWs

A unique aspect of the IPSLS SiNWs in GG mode is that the liquid catalyst drop has two liquid/solid interfaces, that is, the front a-Si:H/In absorption interface and the rear SiNW/In deposition interface, with respective moving velocities of $v_{cm} = J_{out} \cdot \Omega$ and $v_{ma} = J_{in} \cdot \Omega$. The movements of the front and rear interfaces are coupled to each other via the liquid catalyst drop.

Considering a liquid catalyst drop that takes an initial spherical shape with $R_c \approx L_c$ (as energetically preferred for minimizing its surface energy), in order to keep a constant shape during growth, the two liquid/solid interfaces should develop at the same speed (on average) with $v_{cm} \approx v_{ma}$. According to Eq. (5), this requires that

$$\eta \equiv \alpha \cdot R_c \cdot H_a / R_w^2 = \alpha \cdot f^{-1} \cdot H_a / R_c = v_{cm} / v_{ma} \approx 1 \quad (10)$$

with $f = R_w^2 / R_c^2$. As we can see, for a given thickness of the a-Si:H layer H_a (or more specifically the thickness of a-Si:H layer that is absorbed by the catalyst drop), there is only one corresponding size of catalyst drop (R_c^*)

$$R_c^* \equiv \alpha \cdot f^{-1} \cdot H_a \quad (11)$$

that satisfies the balanced condition for the two interfaces and thus allows for a development of a catalyst drop without being *deformed*, as schematically illustrated in Fig. 9(a). In other cases, for a catalyst drop with a size $R_c < R_c^*$ and thus $\eta > 1$ (or $R_c > R_c^*$ thus $\eta < 1$), during the growth, the liquid

catalyst drop will be gradually pushed (pulled) by the rear SiNW/In interface and deform into a shape with $R_c > L_c$ ($R_c < L_c$), as depicted in Fig. 9(b) [Fig. 9(c)]. The deformation of the liquid catalyst drop can be viewed as a reaction to re-establish the equilibrium condition $v_{cm} \approx v_{ma}$ for the two liquid/solid interfaces. Therefore, the catalyst drops of different sizes (and thus experiencing different deformation) will produce SiNWs with different morphologies. Specifically, for the large catalyst drops with $\eta < 1$, when the catalyst drop is stretched by the SiNW/In interface (somewhat lagging behind), the effective cross-section diameter R_c will decrease to return to satisfy $\eta \sim 1$. Under this condition, the SiNWs will also experience a stretching force (exerted by the catalyst) during growth and become straighter. For example, an ultralong (>200 μm) and straight SiNW can be obtained under the condition of $\eta < 1$ and shown in Fig. 1(e), where the SiNW grew out of an ITO pad (where In catalyst drop were formed and thus defined the starting place of the SiNW) and ran into a region with only a-Si:H covering the glass substrate. However, in the extreme case of $\eta \ll 1$ (for very large catalyst drops), a SG growth mode of SiNWs will be preferred, which explains why the SG mode is more commonly adopted by large catalyst drops as seen in Fig. 4. In the opposite case, for small catalyst drops with $\eta > 1$, the catalyst drop is squeezed (pushed from behind), in an attempt to increase R_c to bring back the equilibrium. Interestingly, when the liquid catalyst drop is significantly squeezed, the surface tension could trigger a sudden change in the moving direction of the catalyst drop to restore a spherical shape (favored for minimizing the surface energy), as witnessed in real-time SEM observations.[22] Under this condition, the produced SiNWs are typically bending as indicated in Fig. 9(c). Actually, the adoption of a bending morphology of the SiNW is equivalent to produce a straight but thicker SiNW holding the same c-Si volume, as indicated in Fig. 9(c) by the dashed wire where $R_{w\_eq} > R_w$.

2. Vibration and fine corrugation structures for small perturbations

Under the equilibrium growth condition with $\eta \sim 1$ or with just small perturbations from this condition (with still $\Delta L_c \ll L_{c0}$ and $\Delta R_c \ll R_{c0}$), the catalyst drop can be considered as roughly spherical ($L_{c0} \approx R_{c0}$), with L_{c0} and R_{c0} defined as the corresponding cross-sectional and longitudinal dimensions. Here, since the catalyst drop is not significantly deformed, the effect of the surface tension on a greatly deformed (stretched or squeezed) catalyst drop can be omitted. A simple kinetic equation that takes into account the shape perturbation (in terms of $\Delta L_c \equiv L_c - L_{c0}$ with $L_c = V_c / R_c^2$) and the Si concentration (C_{Si}) at the SiNW/In deposition interface can be established

$$\begin{cases} \dfrac{d\Delta L_c}{dt} = v_{ma} - v_{cm} \\[2mm] \dfrac{dC_{Si}}{dt} = V_c^{-1}\Omega^{-1}(\alpha \cdot v_{ma}H_aR_c - v_{cm}f \cdot R_c^2) \end{cases} \quad (12)$$

with $v_{cm} = J_{out}\Omega = G_{nc}^{-1/2}e^{-G_{nc}/kT} \cdot \Omega$ and $v_{ma} = J_{Si}\Omega = D(C_{eq}^a - C_{Si})/L_c \cdot \Omega$, as defined previously in Eqs. (4) and (5). As-

suming that the small deviations (small perturbations to the equilibrium shape) will not lead to a significant change in C_{Si} in the catalyst drop and thus the nucleation rate J_{out} at SiNW/In interface can be considered approximately as a constant, that is $dv_{cm}/dt=0$, the relations in Eq. (12) can be further simplified into

$$\frac{d^2\Delta L_c}{dt^2} = -\frac{D_s v_{av} R_c^2 f(\eta-1)}{V_c \cdot L_c} = -\frac{f}{\tau_d \tau_m}(\eta-1)L_c, \quad (13)$$

where v_{av} is the average speed (over the whole growth) of the two moving interfaces, $\tau_d \equiv L_c^2/D_s$ and $\tau_m \equiv L_c/v_{av}$ are the typical time scales for the diffusion of Si atoms through the catalyst drop and the movement of the catalyst over a distance equal to its length, respectively. Since $V_c \equiv R_c^2 L_c$ can be considered as a constant during the growth, we have

$$\Delta R_c = -\Delta L_c (R_c/2L_c) \quad (14)$$

and thus

$$\eta - 1 \approx -\frac{\alpha}{f}H_a\frac{\Delta R_c}{R_c^2} = \frac{\alpha}{f}\frac{H_a}{R_c}\frac{\Delta L_c}{L_c} = \eta\frac{\Delta L_c}{L_c}. \quad (15)$$

By inserting Eq. (15) into Eq. (13), it shows that the shape deformation of the liquid catalyst drop, under the small perturbation ($\Delta L_c \ll L_{c0}$), can be described by a harmonic equation as shown below

$$\frac{d^2\Delta L_c}{dt^2} = -\frac{f \cdot \eta}{2\tau_d \tau_m}\Delta L_c. \quad (16)$$

The vibration frequency (ω) and the period (T) of the catalyst drop vibration (in form of $\Delta L_c = \Delta L_{c0}e^{-i\omega t}$) during the growth process can be obtained as

$$\omega = T^{-1} = \sqrt{\frac{f \cdot \eta}{2\tau_d \tau_m}} \sim L_{c0}^{-5/4} \cdot v_{av}^{1/2}. \quad (17)$$

This means that a periodic shape deformation/restoration of the catalyst drop (around the condition of with $\eta \sim 1$) will happen during the growth of GG-SiNWs and thus lead to a periodic corrugation on both the surface of the SiNW and the trench sides with an interval distance of

$$L_{corr} \sim T \times v_{av} = L_{c0}^{5/4} \cdot v_{av}^{1/2} \sim R_w^{5/4} \cdot v_{av}^{1/2}. \quad (18)$$

Meanwhile, the moving rate of GG-SiNWs decreases monotonically with the size of the SiNWs (Fig. 6). If we take the fitting result of the real-time SEM observation data in Fig. 6, $v_{av} \sim R_w^{-0.5\pm0.1}$, the interval between the fine corrugation structure should be

$$L_{corr} \sim R_w^{5/4} \cdot R_w^{-(0.5\pm0.1)/2} \approx R_w^{1.0}. \quad (19)$$

Interestingly, fine corrugation structures can been clearly seen, for example, in the SEM image (of a straight SiNW of 350 nm) shown in the inset of Fig. 10, where the corrugation period L_{corr} is plotted as a function of the diameter of the SiNW R_w. A power-law fitting shows that the corrugation interval increases almost linearly with the diameter of SiNWs $L_{corr} \sim R_w$, which is in excellent agreement with the prediction given in Eq. (19).
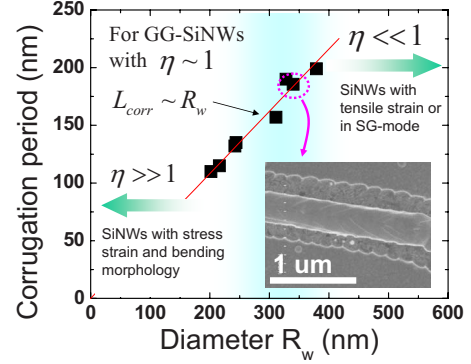
FIG. 10. (Color online) The corrugation period (L_{corr}) as a function of the diameter of the SiNW (R_w) under the condition of small deviations from $\eta \sim 1$. The fine corrugation structures can be seen clearly in the SEM image given in the inset.

In the regions away from the equilibrium condition, that is, $\eta \gg 1$ (left) or $\eta \ll 1$ (right) as indicated by the two arrows in Fig. 10, the liquid catalyst drop is greatly deformed and thus the surface tension will play a significant role in the dynamic interplay between the two interfaces. Under these cases, at least two extra important terms, arising from the surface tension and from the inner viscosity (especially at low temperature), should be taken into account and incorporated in Eq. (12). The growth dynamics under these conditions is too complicated to be adequately addressed by an analytic model (as in the small perturbation case discussed above) and therefore a more comprehensive numerical model should be established, which is beyond the scope of this paper.

It is also worthy to note that there are two major differences between the surface corrugations observed here and the surface facetings formed during the growth of nanowires in VLS mode.[41–43] (1) First, a close examination of the corrugation structures on the IPSLS SiNWs surface, as shown in the inset of Fig. 10, reveals that the morphology, angle, extension, and regularity of spacing of the corrugation patterns on the IPSLS SiNWs are still very different from the typical facetings arising from the termination with [111], [112], or [110] planes[41–43] and (2) second, the corrugation structure exist on both the SiNW sidewall and the trench sides (of the a-Si:H layer) and the corrugations on the a-Si:H trench sides are actually much more prominent, which could not result from the faceting formation on the SiNW sidewall. Though the faceting formation during the growth of crystalline nanowire structures is indeed possible (especially in the finest surface structure), we believe, however, that they are not the major mechanism for the corrugation structure witnessed here. Instead, as we discussed above, the corrugation structure on the IPSLS SiNW is mainly caused by the periodic deformations of the liquid catalyst drop during the IPSLS growth process.

3. Growth dynamics and rolling behavior of SG-SiNWs

The SG-SiNWs provide an instructive and complementary viewpoint of the IPSLS growth mechanism because the two liquid/solid interfaces in SG mode are decoupled and the
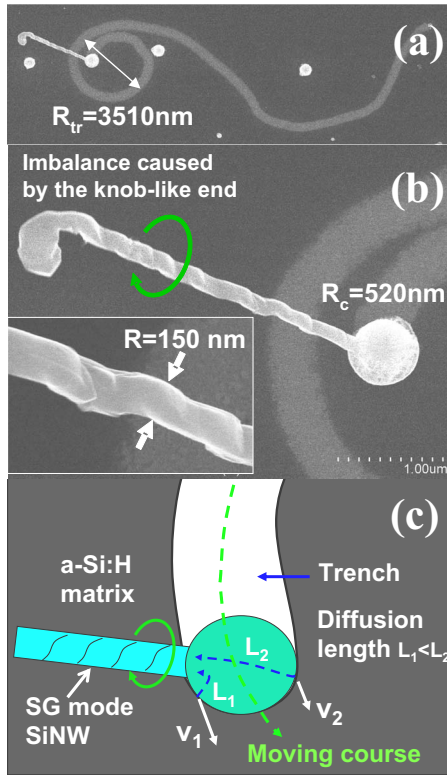
FIG. 11. (Color online) (a) and (b) shows SEM images of a SG-SiNW produced by a large catalyst, which moved around in a spiral trace. The inset of (b) shows the fine structures identified on the SG-SiNW segment. (c) A schematic illustration of the formation process of such spiral path of catalyst drop. v_1 and v_2 stand for the different speeds of the two edge sides of the catalyst absorption interface while L_1 and L_2 are the effective diffusion distances as measured to the deposition interface.

stringent constraint of $v_{cm} \approx v_{ma}$ is relaxed. In Fig. 11, we show a SEM picture of a SG-SiNW (~ 150 nm in diameter) produced by a large catalyst (~ 520 nm in diameter). During its final growth, the catalyst drop followed a nice spiral trace while the SG-SiNW segment always remained on one side of the catalyst drop. It is worth to note that this specific SG-SiNW is indeed a special case among the SG-SiNWs observed. As shown in Figs. 2(d) and 2(e), the typical SG-SiNWs are usually found with irregular shapes and moving paths (as already discussed before). For the SG-SiNW shown in Fig. 11, it seems that a delicate balance, between the weight of suspended SiNW segment and the force exerted by the catalyst drop (which keeps turning in an opposite direction during growth), has been reached. Even though this SG-SiNW is a particular case, it provides many instructive clues and direct information for understanding the mass transport and dynamic behavior happening in the catalyst drop during the growth of the IPSLS SiNWs: (1) first, the common sense would suggest that if the spiral trajectory is *caused* by the gravity force associated to the long SiNW segment, their spiral trajectory should develop to converge on the same side of SiNW. However, as we can see in Fig. 11(a), the catalyst trajectory turns gradually to the opposite side of the SiNW during growth. Actually, the spiral moving path of the catalyst results from the different speeds of the two edge sides of

the catalyst absorption interface ($v_1 > v_2$), as indicated in Fig. 11(c), with v_1 (v_2) being the local speed for the edge side that is close (far) to the deposition SiNW/In interface. According to the diameter of the spiral and the size of the catalyst drop, the different moving speeds for the two edge parts can be roughly estimated

$$\Delta v = v_1 - v_2 = 2 \cdot \bar{v} \cdot R_c/R_{tr} \approx 37 \text{ nm/s} \text{ with } v_2/v_1 \approx 0.7,$$

$$(20)$$

where $\bar{v} = (v_1 + v_2)/2 \approx 103$ nm/s is the average moving rate of the SG-SiNW (as determined by the total length of the trench over the annealing time) and R_{tr} is the diameter of the spiral trace circle. The different moving speeds for the near and far edge sides of the a-Si:H/In interface reflect a difference in the Si incorporation rate at the opposite parts of the absorption edge. According to Eq. (4), with the same C_{eq}^a and C_{Si}, the Si atom incorporation rate (from the a-Si:H/In interface) $v_{ma} = J_{in} \cdot \Omega \sim 1/L_c$, is inversely proportional to the effective diffusion distance (L_c) between the absorption edge and the deposition interface. For the near-edge side, it is a shorter diffusion distance (L_1) to the SiNW/In interface than that seen by the far edge side (L_2) and as a consequence, the local speed (absorption rate) at the near edge is faster than that in the far edge, causing the catalyst to turn toward the *slowly moving side* and develop into a spiral trajectory.

This observation also indicates that the speed of the SG-SiNW is directly determined by the Si atom diffusion flux J_{Si} in the catalyst drop. According to Eq. (4), the diffusion flux J_{Si} is determined by the Si atom concentration difference $\Delta C = C_{eq}^a - C_{Si}$. Since $C_{eq}^a = C_{eq}^c \cdot e^{\Delta E_{ac}/kT}$ can be considered as a constant at the a-Si:H/In interface (determined only by ΔE_{ac} and the temperature), the higher the C_{Si}, the lower the diffusion flux of J_{Si}. As schematically illustrated in Figs. 7(a) and 7(c), C_{Si} is determined by a balance condition between the incoming and the outgoing flux and will decrease with higher nucleation/deposition rate J_{out} at the SiNW end. Thus, the Si atom diffusion flux J_{Si} in the catalyst (which is proportional to the speed of the catalyst drop) is actually limited by the low nucleation/deposition rate at the SiNW/In interface. Therefore, the rate-limiting step here should be the nucleation/deposition rate at the SiNW/In interface, which is intrinsically limited by the Gibbs energy difference between the crystalline and amorphous Si states ΔE_{ac}.

(2) Second, as shown in Fig. 11(b) and in the left inset, fine structures of *helical grooves* with regular spacing are formed along the surface of the SG-SiNW, revealing yet another interesting dynamic behavior. Actually, this screwlike fine structure on the SG-SiNWs is a *faithful* record of the rolling behavior of the catalyst drop. As shown in Fig. 5, when the liquid catalyst drop is drawn by the front absorption edge to move forward on the solid substrate, the friction at its bottom interface is much larger than that of the top surface (totally free). As a consequence, the liquid catalyst drop will adopt a rolling-forward motion instead of sliding on the solid surface, as indicated by the dashed line in Fig. 5, so as to reduce the friction energy during its in-plane movement. For this specific SG-SiNW, we can also see that there is a knoblike butt (formed during the early growth stage) at
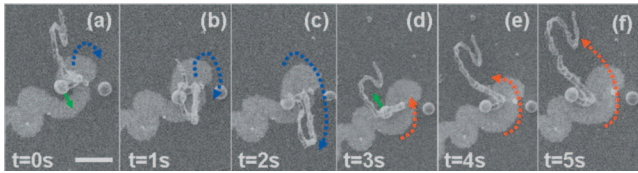
FIG. 12. (Color) A series of six SEM pictures of a single SG-SiNW, during a real-time SEM observation, captured in a sequential order with an interval of 1 s. The green solid arrows indicate the drawing force direction at the absorption interface. The dash arrows in (a)–(c) [(d)–(f)] illustrate the forward (backward) swaying of the SiNWs. The scale bar is 5 μm.

the end of the straight SiNW. During growth, the SiNW was brought into *axial rotation* while the catalyst was rolling forward, as illustrated in Fig. 11(c). This knoblike butt at the end of the SG-SiNW could introduce some imbalances and deviations of deposition interface between the SiNW and the catalyst, leaving these helical groove marks along the side of the produced SiNW.

A direct observation of the rolling behavior of the liquid catalyst drop, as well as the interaction between the SG-SiNW and the catalyst drop, was also achieved in a real-time *in situ* SEM observation of a SiNW growth in a reacting-gas-free annealing process. A series of six SEM pictures of the SG-SiNWs (captured in sequential order with a time interval of 1 s) is presented in Figs. 12(a)–12(f). A long and somewhat bending SG-iNW segment was produced and carried by a catalyst drop of 400 nm in diameter. Interestingly, this SG-SiNW swayed *in space* during the movement of the catalyst drop and served as a real-time *indicator* of the rolling motion of the liquid drop. The catalyst drop kept consuming the a-Si:H and moving around, drawn by the force exerted at the front absorption interface as indicated by the green arrows in Figs. 12(a) and 12(d). From Figs. 12(a)–12(c), the SG-SiNW was *swung* from an up-standing position gradually (over around 90°) to *touch* on the substrate surface, as illustrated by the blue dash arrow. Then, due to the change in the effective absorption edge, in Figs. 12(c)–12(f), the SG-SiNW was swayed back to a up standing, this reverse motion [as opposite to that in Figs. 12(a)–12(c)] is depicted by the red dash arrows. Meanwhile, the growing SG-SiNW carried by catalyst drop also imposed constraints on the movement of the catalyst and led to a very irregular moving course. It is noteworthy that, though the hydrodynamic details in the liquid catalyst drop are too com-

plicated to be addressed in this paper, these observations provide an indication for the existence of a convectionlike circulation in the liquid catalyst drop, as illustrated in Fig. 5.

IV. SUMMARY AND CONCLUSION

In summary, we have presented an in-depth investigation of the IPSLS growth of SiNWs. In particular, we have discussed: (1) the major steps involved in the IPSLS process: (i) the absorption of Si atoms from a-Si:H matrix into the In catalyst, (ii) the mass transport through the catalyst drop, and (iii) the deposition as crystalline SiNWs.

(2) We have studied the size and temperature dependences of the SiNWs growth rate and identified two growth modes of the IPSLS SiNWs: the GG and SG modes, which provide important comparative viewpoints for understanding the growth mechanism. We found that (i) the diameter of SiNW is proportional to the diameter of the guiding catalyst drop; (ii) the growth of SiNWs (in both the GG or SG mode) is a thermally activated process, with an activation energy of ~1 eV; (iii) the grow rate of GG-SiNWs is limited by the nucleation/deposition step at the SiNW/In interface and decreases with the diameter of the SiNWs; and (iv) the moving rate of SG-SiNWs is determined by the mass transport process in the catalyst drop and scales up with the diameter of SiNWs.

(3) We show that the interplays between the front absorption and the rear deposition interfaces (both are liquid/solid interfaces) play a determining role in controlling the morphology of the produced SiNWs. The observed periodic surface corrugation on both the SiNW and the a-Si:H trench sides resulted from a periodic vibrating behavior of the liquid catalyst drop during the growth, which can be modeled by a kinetic equation describing the coupling between the two interfaces.

(4) Furthermore, direct experimental evidences obtained in real-time SEM observations have been provided, which support the assumed rolling-forward movement of the liquid In catalyst drop during the in-plane SiNW growth.

These results provide an important basis for achieving a comprehensive understanding of the unique IPSLS growth mechanism and reveal yet the rich dynamics and physics of the nanoscaled solid-liquid-solid system, which could have broad and important implications to both the applied and fundamental researches.

[1] C. M. Lieber, Mater. Res. Bull. **28**, 486 (2003).

[2] L. Wei and M. L. Charles, J. Phys. D **39**, R387 (2006).

[3] Y. Cui, Z. Zhong, D. Wang, W. U. Wang, and C. M. Lieber, Nano Lett. **3**, 149 (2003).

[4] J. F. Qi, A. M. Belcher, and J. M. White, Appl. Phys. Lett. **82**, 2616 (2003).

[5] A. I. Hochbaum, R. K. Chen, R. D. Delgado, W. J. Liang, E. C. Garnett, M. Najarian, A. Majumdar, and P. D. Yang, Nature (London) **451**, 163 (2008).

[6] Y. Huang, X. Duan, Q. Wei, and C. M. Lieber, Science **291**, 630 (2001).

[7] R. S. Wagner and W. C. Ellis, Appl. Phys. Lett. **4**, 89 (1964).

[8] Y. Cui, L. J. Lauhon, M. S. Gudiksen, J. Wang, and C. M. Lieber, Appl. Phys. Lett. **78**, 2214 (2001).

[9] Y. Wu, Nano Lett. **4**, 433 (2004).

[10] A. Colli, A. Fasoli, P. Beecher, P. Servati, S. Pisana, Y. Fu, A. J. Flewitt, W. I. Milne, J. Robertson, C. Ducati, S. De Franceschi, S. Hofmann, and A. C. Ferrari, J. Appl. Phys. **102**, 034302

(2007).

[11] J. F. Dayen, A. Rumyantseva, C. Ciornei, T. L. Wade, J. E. Wegrowe, D. Pribat, and C. S. Cojocaru, Appl. Phys. Lett. **90**, 173110 (2007).

[12] Y. Shan and S. J. Fonash, ACS Nano **2**, 429 (2008).

[13] R.-Q. Zhang, Y. Lifshitz, and S. T. Lee, Adv. Mater. (Weinheim, Ger.) **15**, 635 (2003).

[14] N. Wang, Y. H. Tang, Y. F. Zhang, C. S. Lee, and S. T. Lee, Phys. Rev. B **58**, R16024 (1998).

[15] L. Eun Kyung, C. Byoung Lyong, P. Yong Dae, K. Young, K. Sun Young, and K. Hyeong Joon, Nanotechnology **19**, 185701 (2008).

[16] A. T. Heitsch, D. D. Fanfair, H.-Y. Tuan, and B. A. Korgel, J. Am. Chem. Soc. **130**, 5436 (2008).

[17] J. Bae, N. N. Kulkarni, J. P. Zhou, J. G. Ekerdt, and C.-K. Shih, J. Cryst. Growth **310**, 4407 (2008).

[18] J. Arbiol, B. Kalache, P. Roca i Cabarrocas, J. R. Morante, and A. Fontcuberta i Morral, Nanotechnology **18**, 305606 (2007).

[19] L. Yu, P.-J. Alet, G. Picardi, I. Maurin, and P. Roca i Cabarrocas, Nanotechnology **19**, 485605 (2008).

[20] P.-J. Alet, L. Yu, G. Patriarche, S. Palacin, and P. Roca i Cabarrocas, J. Mater. Chem. **18**, 5187 (2008).

[21] H. F. Yan, Y. J. Xing, Q. L. Hang, D. P. Yu, Y. P. Wang, J. Xu, Z. H. Xi, and S. Q. Feng, Chem. Phys. Lett. **323**, 224 (2000).

[22] L. Yu, P.-J. Alet, G. Picardi, and P. Roca i Cabarrocas, Phys. Rev. Lett. **102**, 125501 (2009).

[23] O. Nast, T. Puzzer, L. M. Koschier, A. B. Sproul, and S. R. Wenham, Appl. Phys. Lett. **73**, 3214 (1998).

[24] L. Pereira, P. Barquinha, E. Fortunato, and R. Martins, Thin Solid Films **487**, 102 (2005).

[25] E. Nygren, A. P. Pogany, K. T. Short, J. S. Williams, R. G. Elliman, and J. M. Poate, Appl. Phys. Lett. **52**, 439 (1988).

[26] A. U. Cosckun, Y. Yener, and F. Arinc, Modell. Simul. Mater. Sci. Eng. **10**, 539 (2002).

[27] M. Kimura, N. DJilali, S. Dost, H. Kanai, A. Tanaka, and T. Sukegawa, J. Cryst. Growth **167**, 516 (1996).

[28] L. Yu, M. Oudwan, O. Moustapha, F. Franck, and P. Roca i Cabarrocas, Appl. Phys. Lett. **95**, 113106 (2009).

[29] L. Yu and P. Roca i Cabarrocas, Phys. Rev. B **80**, 085313 (2009).

[30] I. Stich, R. Car, and M. Parrinello, Phys. Rev. B **44**, 11092 (1991).

[31] S. Roorda, S. Doorn, W. C. Sinke, P. M. L. O. Scholte, and E. van Loenen, Phys. Rev. Lett. **62**, 1880 (1989).

[32] W. A. Tiller, *The Science of Crystallization: Microscopic Interfacial Phenomena* (Cambridge University Press, New York, 1991).

[33] V. G. Dubrovskii, N. V. Sibirev, G. E. Cirlin, J. C. Harmand, and V. M. Ustinov, Phys. Rev. E **73**, 021603 (2006).

[34] V. G. Dubrovskii and N. V. Sibirev, Phys. Rev. E **70**, 031604 (2004).

[35] B. A. Wacaser, K. A. Dick, J. Johansson, M. T. Borgström, K. Deppert, and L. Samuelson, Adv. Mater. (Weinheim, Ger.) **21**, 153 (2009).

[36] T. R. Anthony and H. E. Cline, J. Appl. Phys. **43**, 2473 (1972).

[37] W. C. Yang, H. Ade, and R. J. Nemanich, Phys. Rev. B **69**, 045421 (2004).

[38] L. Yu, B. O'Donnell, P. J. Alet, and P. Roca i Cabarrocas (unpublished).

[39] K.-K. Lew and J. M. Redwing, J. Cryst. Growth **254**, 14 (2003).

[40] H. Jeong, T. E. Park, H. K. Seong, M. Kim, U. Kim, and H. J. Choi, Chem. Phys. Lett. **467**, 331 (2009).

[41] F. Li, P. D. Nellist, and D. J. H. Cockayne, Appl. Phys. Lett. **94**, 263111 (2009).

[42] B. A. Korgel, Nature Mater. **5**, 521 (2006).

[43] F. M. Ross, J. Tersoff, and M. C. Reuter, Phys. Rev. Lett. **95**, 146104 (2005).